Syntheses of Three-Port DC–DC Converters

Peng Luo, Tsorng-Juu Liang, *Fellow, IEEE*, Kai-Hui Chen, Shih-Ming Chen, and Jiann-Fuh Chen, *Fellow, IEEE*

***Abstract*—This article proposes a systematic method to construct three-port converters (TPCs) and bidirectional three-port converters (BTPCs) by integrating two dc–dc converters including nonisolated and isolated types. By adding extra one power switch and one diode, the TPCs can be constructed by the dc–dc converters. A series of the proposed TPCs can provide independent power flow control of single-input to single-output, single-input to dual-output, and dual-input to single-output. By adding extra two power switches, the BTPCs can be constructed by the dc–dc converters. The power flows between any two ports can be controlled bidirectionally without significantly altering their architecture. Finally, a typical nonisolated BTPC is analyzed and implemented with rated power of 300 W and three ports voltages of 48, 72, and 200 V to verify the feasibility and effectiveness of the theoretical analyses. The highest measured efficiency is 98.4%.**

***Index Terms*—Bidirectional converter, energy storage, renewable energy, three-port converter (TPC).**

I. Introduction

THREE-PORT converters (TPCs) have recently gained popularity in sustainable energy system (SUS), such as wind power and solar power, and energy storage system (ESS), which can ensure a continuous and stable power supply for the load [1], [2], [3], [4], [5], [6], [7], [8], [9], [10], [11], [12], [13], [14], [15], as shown in Fig. 1(a). For multiple ESSs applications, the bidirectional power flows among ESSs and dc bus are required, as shown in Fig. 1(b) [16], [17], [18], [19], [20], [21], [22], [23], [24], [25], [26], [27], [28], [29], [30], [31]. Traditionally, three independent unidirectional dc–dc converters are employed to interface source port V_S, battery port V_B, and load port V_L, as shown in Fig. 2. However, components cannot be shared among three ports, resulting in high cost and low efficiency. To address the problem, many researches on TPCs have been done regarding topology derivations for various applications.

Based on coupled inductor and voltage double techniques, the nonisolated TPCs have been presented [2], [3]. However, it suffers from the cross-regulation problem with multiple power flow conditions. By using three inductors, the power flows of the single-input–dual-output (SIDO) modes can be controlled independently, thus the cross regulation problem is solved [4]. By integrating a coupled inductor with three power switches, the boost-flyback and switched-capacitor techniques are used to transfer energy from photovoltaic (PV) to output and battery to output, respectively [5]. However, the power flows from PV to battery and load are coupled. TPC can also be constructed by integrating switched capacitor converter, bidirectional pulsewidth modulation (PWM) converter, and series-resonant converter, but more power switches and complex control are used [6]. The number of power switches was reduced by integrating a bidirectional converter for TPC [7]. For dual-input sources operation, the quadratic boost technique is used to form a TPC with reduced device counts to achieve high stepup [8]. However, the control is complex.

For safety requirements, the multiple windings with galvanic isolation transformer are used for isolated TPC. Isolated TPCs with high-power capacity was presented based on dual active bridge with a third winding and rectifier output, but

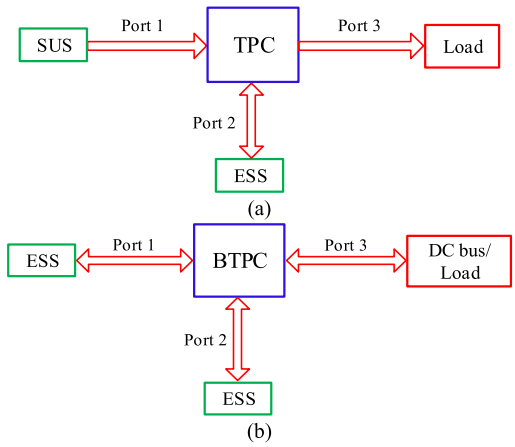

Fig. 1. Applications of (a) TPC in SUS and ESS and (b) BTPC in multiple ESSs.

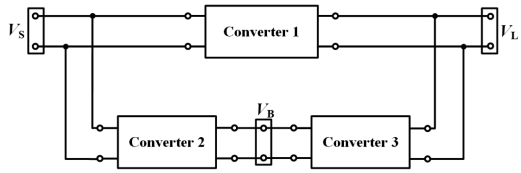

Fig. 2. Conventional SUS and ESS systems with three converters.

Manuscript received 13 April 2023; revised 6 July 2023; accepted 15 August 2023. Date of publication 4 September 2023; date of current version 23 October 2023. This work was supported by National Science and Technology Council (NSTC), Taiwan, under Grant 110-2221-E-006-123-MY3. Recommended for publication by Associate Editor S. Kapat. *(Corresponding author: Tsorng-Juu Liang.)*

Peng Luo is with the Guangdong Ocean University, Zhanjiang 524088, China (e-mail: luopeng@gdou.edu.cn).

Tsorng-Juu Liang, Kai-Hui Chen, Shih-Ming Chen, and Jiann-Fuh Chen are with the Electrical Engineering, National Cheng Kung University, Tainan 70101, Taiwan (e-mail: tjliang@mail.ncku.edu.tw; z10810040@ncku.edu.tw; smchen@ncku.edu.tw; chenjf@mail.ncku.edu.tw).

Color versions of one or more figures in this article are available at https://doi.org/10.1109/TPEL.2023.3309892.

Digital Object Identifier 10.1109/TPEL.2023.3309892

more power switches are used [9]. Isolated TPC with simple control scheme was composed of a Z-source boost converter and coupled inductor with voltage doubler, but more components are used and full-load efficiency is low [10]. By integrating boost and dual switches buck–boost converters [11], interleaved boost converter [12], and switched-capacitor technology [13] with LLC converter, isolated TPCs can achieve higher efficiency; however, the power managements among three ports become complex. The single magnetic core isolated TPC was formed by integrating bidirectional PWM converter and SRC, but the energy from battery to output needs twice power transferring processes [14]. Isolated TPC was presented with two interleaved flyback–forward converters; however, the power flow control in SIDO is complex [15]. By integrating full-bridge cell with a three-winding transformer [16], [17], [18] and a boost converter [19], isolated TPCs were presented with more power switches and complex control.

In combining a full-bridge inverter, a conventional boost, and a bidirectional single inductor converter, a nonisolated bidirectional three-port converter (BTPC) was presented [21]. A simple nonisolated BTPC composed of a boost converter and a bidirectional buck/boost converter with two power switches and two inductors was presented, but the energy from PV to battery needs twice power transferring processes [22].

With four power switches, the nonisolated BTPCs can be formed by two conventional bidirectional buck–boost converters in parallel or in series; however, twice power transferrings are required for the energy transferings between the battery and dc bus, and from PV to battery, respectively, [23]. Two nonisolated BPTCs can be constructed by integrating two bidirectional buck–boost converters [24] or two bidirectional buck converters [25]. However, the time-multiplexing control scheme in SIDO stage is required. Four phase bidirectional buck–boost with coupled inductor was presented [26]. But more power switches are adopted.

Isolated BTPCs can be built by integrated three full-bridge cells with one transformer [27], [28], [29], [30]. However, more power switches are used and control scheme is complicated. By using the boost flyback, and forward converters, an isolated BTPC was formed by sharing the power switches [31]. However, it is difficult to control power flows independently among two batteries and load.

The simple syntheses of the nonisolated TPCs were presented by adding one power switch and one diode in between two sources with two conventional converters [32]. By an additional one power switch and one diode with the conventional converter, the nonisolated TPC was revealed [33]. The syntheses of integrating SIDO converters, dual-input–single-output (DISO) dc–dc converters, and converters with single inductor for multiple-intput and multiple-output were revealed [34], [35], [36], [37]. However, the energy transferings between source(s) and load(s) are unidirectional. By integrating two power switches and inductor/transformer, the bidirectional nonisolated converter for battery port and unidirectional isolated converter for load were addressed [38]. A family of BTPCs was presented by adding two bidirectional buck–boost converters with cascaded structure [39].

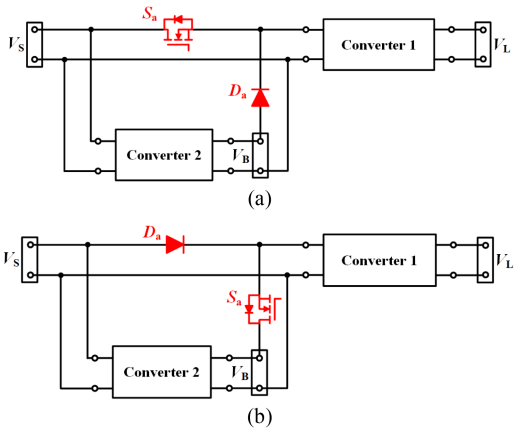

Fig. 3. Topology syntheses for constructing TPCs. (a) Integrate TPC under $V_S > V_B$. (b) Integrate TPC under $V_S < V_B$.

In this article, TPCs are derived systematically by adding additional one power switch and one diode. The power flows of the constructed TPCs are controlled independently from SUS to ESS/load and ESS to load. Also, by adding two power switches in connecting two dc–dc converters, BTPCs are formed analytically. The power flows among SUS, ESS, and dc bus can be controlled independently by the presented BTPCs. These TPCs and BTCs are needed to attain suitable operation ranges for different voltage applications in power systems.

II. Syntheses and Topology Derivations of TPCs and BTPCs

To integrate a TPC with two converters, additional power switch S_a and diode D_a are used to achieve power flows, as shown in Fig. 3. To avoid the shorted circuit of source and battery, power switch S_a is connected to source and power diode D_a is connected to battery when $V_S > V_B$ as shown in Fig. 3(a). When $V_S < V_B$, power diode D_a is connected to source and power switch S_a is connected to battery as shown in Fig. 3(b).

By replacing the diode with power switch in Fig. 3, the bidirectional power flows can be performed. Nonisolated BTPCs and isolated BTPCs composed of two battery ports V_{B1} and V_{B2}, and a dc-bus port V_{Bus} can be derived by combing the two bidirectional converters with two additional power switches, as shown in Fig. 4. When $V_{B1} > V_{B2}$, drain terminal of S_{a1} is connected to V_{B1}, source terminal of S_{a2} is connected to V_{B2}, and source terminal of S_{a1} and drain terminal of S_{a2} are common connected to converter 2. When $V_{B2} > V_{B1}$, source terminal of S_{a1} is connected to V_{B1}, drain terminal of S_{a2} is connected to V_{B2}, and drain terminal of S_{a1} and source terminal of S_{a2} are common connected to converter 2. By setting ON/OFF of S_{a1} and S_{a2}, the energy transfers from V_{B1} to V_{Bus} and V_{B2} to V_{Bus} can be controlled independently, as shown in Fig. 4(a) and (b). The voltage stress on power switches S_{a1} and S_{a2} is $|V_{B1}\text{-}V_{B2}|$. In order to keep the two port voltages of converters with the same reference point in Figs. 3 and 4, converter 2 must be common ground.

In order to illustrate the synthesis of TPC, based on the five basic converters, namely buck, boost, buck–boost, flyback, and

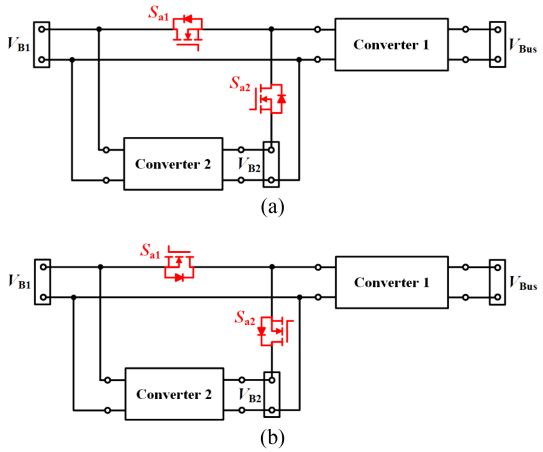

Fig. 4. Topology syntheses for constructing BTPCs. (a) Integrate BTPC under $V_{B1} > V_{B2}$. (b) Integrate BTPC under $V_{B1} < V_{B2}$.

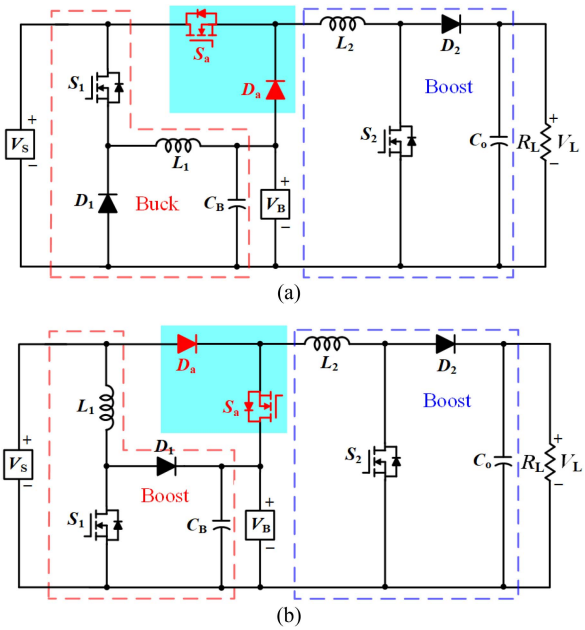

Fig. 5. Nonisolated TPCs under (a) $V_L > V_S > V_B$ (buck + boost) and (b) $V_L > V_B > V_S$ (boost + boost).

forward, nonisolated TPCs and isolated TPCs can be derived by combing the two basic converters.

Nonisolated TPCs: When $V_L > V_S > V_B$, buck converter and boost converter are used to construct TPC. The buck converter is used to transfer energy from V_S to V_B, and the boost converter is used to provide energy to load from source and battery as shown in Fig. 5(a). When V_S provides energy to V_L, additional power switch S_a, is always ON and additional diode D_a is used to avoid shorted circuit of V_S and V_B. When V_B provides energy to V_L, additional power switch S_a is always OFF to block the energy from V_S to V_L. Then, the energy transferring from either V_S or V_B to V_L can be controlled independently. When V_S provides energy to V_B and V_L, additional power switch S_a is always ON, and S_1 and S_2 are controlled independently to regulate the power from V_S to V_B and V_L, respectively. When $V_L > V_B > V_S$, two

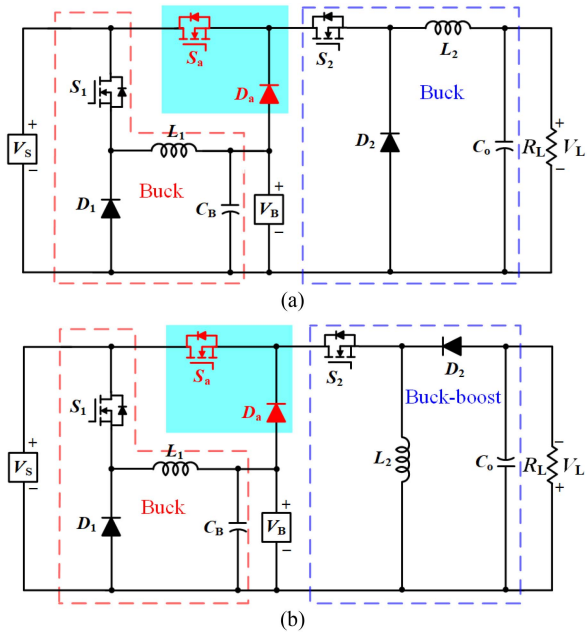

Fig. 6. Under $V_S > V_B$, two integrated nonisolated TPCs with (a) buck + buck and (b) buck + buck boost.

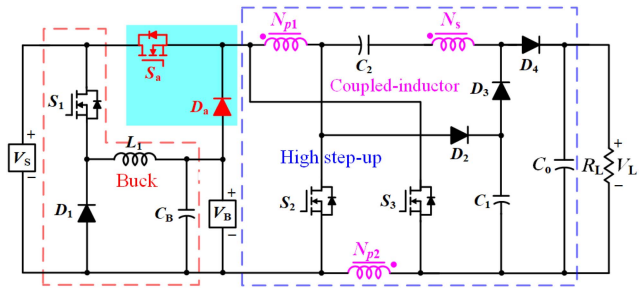

Fig. 7. One integrated nonisolated TPCs with buck converter and high-step-up converter.

boost converters are used to convert energy from V_S to V_B, V_B to V_L, and V_S to V_L, as shown in Fig. 5(b). When only V_S provides energy to V_L, S_a is always OFF. S_a is always ON when only V_B provides energy to V_L. Since $V_B > V_S$, the OFF/ON of S_a and diode D_a are used to ensure that there is only one source providing energy to V_L independently.

Similarly, as shown in Fig. 6(a), when $V_S > V_B > V_L$, two buck converters are used to construct TPC with additional power switch and diode. When $V_S > V_B$, one buck converter and one buck–boost converter are used to convert energy among V_S, V_B, and V_L, as shown in Fig. 6(b).

To demonstrate the generality of the proposed topology synthesis, in Fig. 5(a), by replacing the boost converter with high step-up converter in [40], a nonisolated TPC with high-voltage gain is shown in Fig. 7. Assuming the winding ratios of N_{p1}, N_{p2}, and N_s of the coupled inductor are $1:1:n$, and D is the duty cycle of synchronous switches S_2 and S_3, the voltage gain from V_S or V_B to V_L is written as

$$\frac{V_L}{V_S} = \frac{3+n+D}{1-D} \quad \text{or} \quad \frac{V_L}{V_B} = \frac{3+n+D}{1-D}. \tag{1}$$

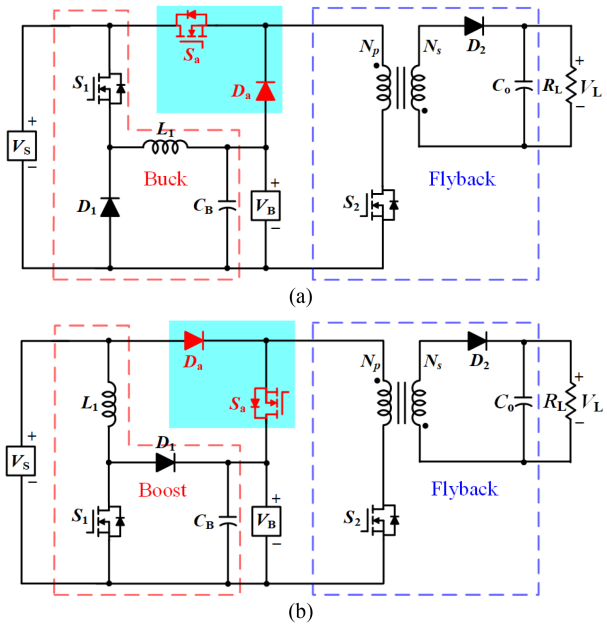

Fig. 8. Isolated TPCs under (a) $V_S > V_B$ (buck + flyback) and (b) $V_S < V_B$ (boost + flyback).

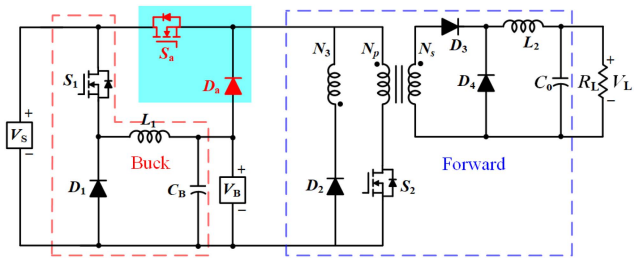

Fig. 9. Isolated TPC with buck and forward converters under $V_S > V_B$.

Isolated TPCs: When $V_S > V_B$, buck converter and flyback converter are used to construct isolated TPC. The buck converter is used to transfer energy from V_S to V_B. As shown in Fig. 8(a), the flyback converter is used to provide energy to load from V_S and V_B by controlling power switch S_a always ON and OFF, respectively. Then, the energy transferring from either V_S or V_B to V_L can be controlled independently. When V_S provides energy to V_B and V_L, power switch S_a is always ON, and S_1 and S_2 are controlled independently to regulate the power from V_S to V_B and V_S to V_L, respectively.

Similarly, when $V_S < V_B$, the boost converter is used to convert energy from V_S to V_B, and the flyback converter is used to convert energy from V_S to V_L and V_B to V_L, as shown in Fig. 8(b). The power transferrings among V_L, V_B, and V_S are controlled independently. By the same concept, the forward converter can also be adopted for the energy transfers from V_S to V_L and V_B to V_L, as shown in Fig. 9.

Based on Fig. 3, integrating a buck converter and an isolated soft-switching high-step-up converter in [41], an isolated TPC is shown in Fig. 10. From V_S or V_B to V_L, S_2 and S_3 can achieve zero-voltage switching.

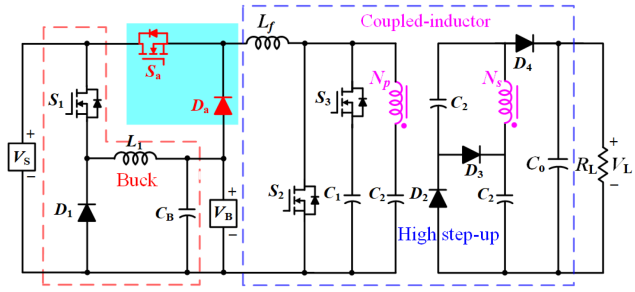

Fig. 10. One integrated isolated TPCs with buck converter and soft-switching high step-up converter $V_S > V_B$.

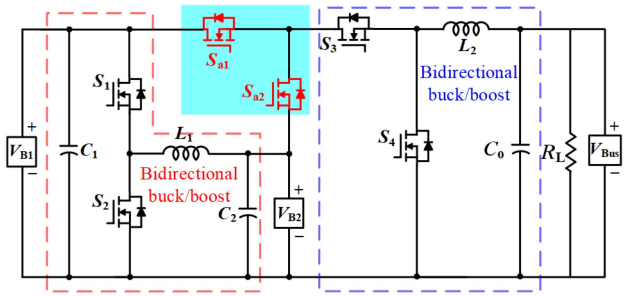

Fig. 11. Nonisolated BTPC with bidirectional buck/boost and buck/boost converters under $V_{B1} > V_{B2} > V_{Bus}$.

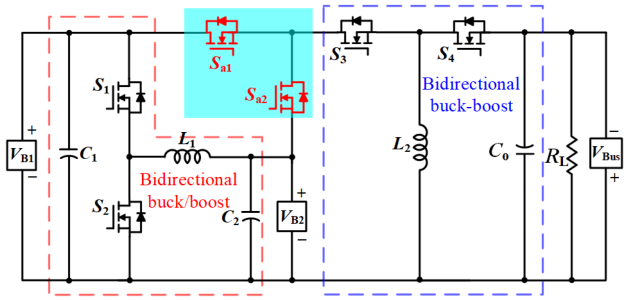

Fig. 12. Nonisolated BTPC with bidirectional buck/boost and buck–boost converters under $V_{B1} > V_{B2}$.

Nonisolated BTPCs: When $V_{B1} > V_{B2} > V_{Bus}$, two bidirectional buck/boost converters are used to construct BTPC, as shown in Fig. 11. The bidirectional buck/boost converter constructed by S_1, S_2, and L_1 is used to transfer energy between V_{B1} and V_{B2} while S_{a1} and S_{a2} are always OFF. By setting ON/OFF of S_{a1} and S_{a2}, the bidirectional buck/boost converter constructed by S_3, S_4, and L_2 is used to transfer energy between V_{B1} and V_{BUS}, and V_{B2} and V_{BUS}. When energy is transferred between V_{B2} and V_{Bus}, power switch S_{a1} is always OFF to block the energy from V_{B1} to V_{Bus}. When energy is transferred between V_{B1} and V_{Bus}, power switch S_{a2} is always OFF to avoid shorted circuit of V_{B1} and V_{B2}, and also block the energy from V_{Bus} to V_{B2}. Then, the power transferring among V_{B1}, V_{B2}, and V_{Bus} are controlled independently.

Similarly, as shown in Fig. 12, when $V_{B1} > V_{B2}$, one bidirectional buck/boost converter and one bidirectional buck–boost converters are used to construct BTPC with two additional power switches.

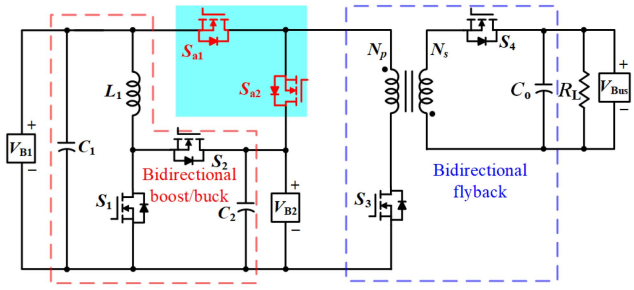

Fig. 13. Isolated BTPC with bidirectional boost/buck and flyback converters under $V_{B1} > V_{B2}$.

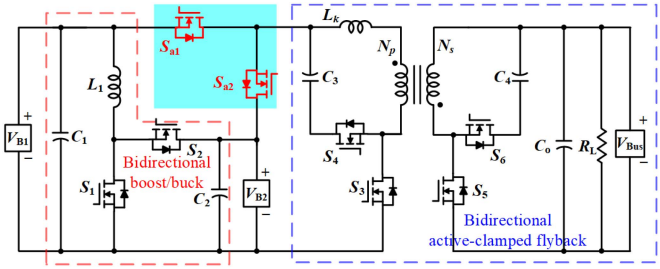

Fig. 14. Isolated BTPC with bidirectional boost/buck and active-clamped flyback converters under $V_{B1} > V_{B2}$.

Isolated BTPCs: When $V_{B2} > V_{B1}$, bidirectional boost/buck converter and bidirectional flyback converter are used to construct BTPC, as shown in Fig. 13.

When energy is transferred between V_{B1} and V_{B2}, power switches S_{a1} and S_{a2} are always OFF to avoid energy transfers between V_{B1} and V_{BUS}, and V_{B2} and V_{BUS}. The bidirectional flyback converter is used to transfer energy between V_{B1} and V_{Bus}, power switch S_{a1} is always ON and S_{a2} is always OFF. When energy is transferred between V_{B2} and V_{Bus} by the bidirectional flyback converter, power switch S_{a1} is always OFF and S_{a2} is always ON to block the energy transfer between V_{B1} and V_{Bus}. Then, the power transferrings among V_{B1}, V_{B2}, and V_{Bus} are controlled independently. Moreover, integrating a bidirectional boost/buck converter and a bidirectional active-clamped flyback converter in [42], an isolated BTPC is presented in Fig. 14. V_{B1} and V_{B2} are isolated from V_{Bus}. Since the power switches can achieve soft-switching when the energy is transferred with V_{Bus}, the switching frequency can be increased for reducing the transformer size.

III. Analyses and Design of Nonisolated BTPC

The BTPC composed of bidirectional buck/boost converter and boost/buck converter is analyzed and designed to build the experimental prototype for verification of the proposed synthesis method, as shown in Fig. 15. Where additional switches S_{a1} and S_{a2} are added to form the bidirectional energy transfers between V_{B1} and V_{B2}, V_{B1} and V_{Bus}, and V_{B2} and V_{Bus}. To simply the analyses, the following conditions are assumed.

1) MOSFETs are ideal, except the body diode of MOSFETs is considered.

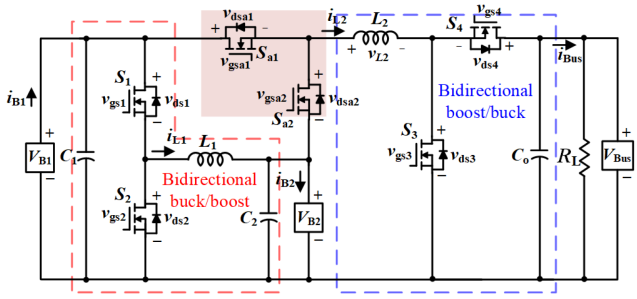

Fig. 15. Nonisolated BTPC with bidirectional buck/boost and boost/buck converters under $V_{Bus} > V_{B1} > V_{B2}$.

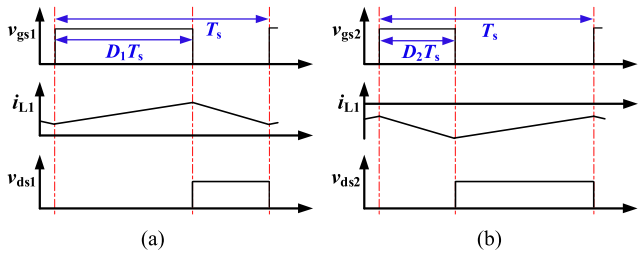

Fig. 16. Key waveforms for Stage I. (a) V_{B1} to V_{B2} (buck). (b) V_{B2} to V_{B1} (boost).

2) The proposed converter is operated at steady state under continuous conduction mode (CCM) conditions.
3) The voltages of the three ports are defined as $V_{Bus} > V_{B1} > V_{B2}$.
4) D_1, D_2, D_3, and D_4 are defined as the duty ratios of S_1, S_2, S_3, and S_4, respectively.

Five stages are discussed in the following sections.

A. Stage I: Power Flows Between V_{B1} and V_{B2} ($P_{B1} = P_{B2}$)

In this stage, switches S_{a1}, S_{a2}, S_3, and S_4 are OFF. The bidirectional buck/boost converter is used to transfer the energy between V_{B1} and V_{B2}, with key waveforms, as shown in Fig. 16. S_1 and S_2 act as the main switch when V_{B1} provides energy to V_{B2} with buck converter, and V_{B2} provides energy to V_{B1} with boost converter, respectively. Then, the voltage conversion ratios can be derived as follows:

$$V_{B2} = D_1 V_{B1}. \tag{2}$$

$$V_{B1} = \frac{1}{1 - D_2} V_{B2}. \tag{3}$$

B. Stage II: Power Flows Between V_{B1} and V_{Bus} ($P_{B1} = P_{Bus}$)

In this stage, switches S_1, S_2, and S_{a2} are turned OFF. The bidirectional boost/buck converter is used to transfer the energy between V_{B1} and V_{Bus}, with key waveforms, as shown in Fig. 17. S_3 and S_4 act as the main switch when V_{B1} provides energy to V_{Bus} with boost converter, and V_{Bus} provides energy to V_{B1} with buck converter, respectively. Then, the voltage conversion

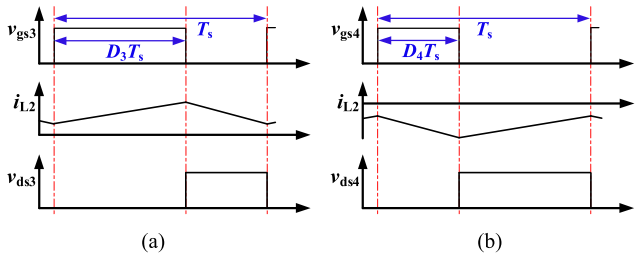

Fig. 17. Key waveforms for Stage II. (a) V_{B1} to V_{Bus} (boost). (b) V_{Bus} to V_{B1} (buck).

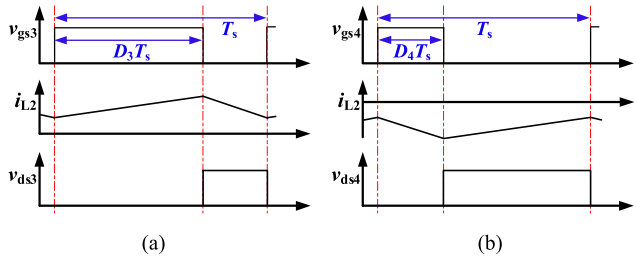

Fig. 18. Key waveforms for Stage III. (a) V_{B2} to V_{Bus} (boost). (b) V_{Bus} to V_{B2} (buck).

ratios can be derived as follows:

$$V_{\mathrm{Bus}} = \frac{1}{1-D_3}\, V_{\mathrm{B1}} \tag{4}$$

$$V_{\mathrm{B1}} = D_4\, V_{\mathrm{Bus}}. \tag{5}$$

C. Stage III: Power Flows Between V_{B2} and V_{Bus} ($P_{B2} = P_{Bus}$)

In this stage, S_1, S_2, and S_{a1} are turned OFF. The bidirectional boost/buck converter is used to transfer the energy between V_{B2} and V_{Bus}, with key waveforms, as shown in Fig. 18. S_3 and S_4 act as the main switch when V_{B2} provides energy to V_{Bus} with boost converter, and V_{Bus} provides energy to V_{B2} with buck converter, respectively. Then, the voltage conversion ratios can be derived as follows:

$$V_{\mathrm{Bus}} = \frac{1}{1-D_3}\, V_{\mathrm{B2}} \tag{6}$$

$$V_{\mathrm{B2}} = D_4\, V_{\mathrm{Bus}}. \tag{7}$$

D. Stage IV: Power Flows From V_{B2} to V_{B1} and V_{Bus} ($P_{B2} = P_{B1} + P_{Bus}$)

In this stage, V_{B2} simultaneously provides energy to V_{B1} and V_{Bus}. S_{a2} is always turned ON, and S_{a1} is always turned OFF. S_2 and S_3 are the main switches regulating the power from V_{B2} to V_{B1} and from V_{B2} to V_{Bus}, respectively. There is no energy transfer between V_{B1} and V_{Bus}. Thus, it can transfer energy from one input to two outputs with independent power flow control. The relationships between V_{B2} and V_{B1}, V_{Bus} are the same as (3) and (6).

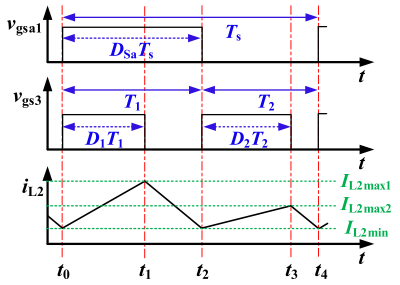

Fig. 19. Key waveforms from V_{B1} and V_{B2} to V_{Bus}.

E. Stage V: Power Flows From V_{B1} and V_{B2} to V_{Bus} ($P_{B2} + P_{B1} = P_{Bus}$)

In this stage, switches S_1 and S_2 are always turned OFF, and S_{a1} and S_3 are the main switches. Combing power flows from V_{B1} to V_{Bus} and V_{B2} to V_{Bus}, and applying interleaved control methods, V_{B1} and V_{B2} transfer energy to V_{Bus} independently, as shown in Fig. 19. From moments t_0 to t_2, S_{a1} is ON and V_{B1} provides energy to V_{Bus}. From moments t_2 and t_4, S_{a1} is OFF and V_{B2} provides energy to V_{Bus}.

Under CCM, in Fig. 19, during $(1-D_1)T_1$, the charge of L_2 is obtained as the following:

$$Q_1 = \frac{1}{2}\,(1-D_1)\,T_1\left[I_{L2\mathrm{min}} + \left(\frac{V_{\mathrm{B1}}}{L_2}D_1T_1 + I_{L2\mathrm{min}}\right)\right]. \tag{8}$$

Also, during $(1-D_2)T_2$, the charge of L_2 is obtained as follows:

$$Q_2 = \frac{1}{2}\,(1-D_2)\,T_2\left[I_{L2\mathrm{min}} + \left(\frac{V_{\mathrm{B2}}}{L_2}D_2T_2 + I_{L2\mathrm{min}}\right)\right]. \tag{9}$$

During 0-T_{S}, by using charge balance of L_2, the following can be derived:

$$Q_1 + Q_2 = I_{\mathrm{Bus}}\, T_{\mathrm{S}} \tag{10}$$

Substituting (8) and (9) into (10), $I_{L2\mathrm{min}}$ can be derived as

$$I_{L2\mathrm{min}} = \frac{2I_{\mathrm{Bus}}T_S - \frac{V_{\mathrm{B1}}}{L_2}D_1\,(1-D_1)\,T_1^2 - \frac{V_{\mathrm{B2}}}{L_2}D_2\,(1-D_2)\,T_2^2}{2\,(1-D_1)\,T_1 + 2\,(1-D_2)\,T_2}. \tag{11}$$

The average currents flowing through V_{B1} and V_{B2} are derived as follows:

$$I_{\mathrm{B1}} = \frac{V_{\mathrm{B1}}}{2L_2}\,D_1T_1 + I_{L2\mathrm{min}} \tag{12}$$

$$I_{\mathrm{B2}} = \frac{V_{\mathrm{B2}}}{2L_2}\,D_2T_2 + I_{L2\mathrm{min}}. \tag{13}$$

From (12) and (13), the ratio of the power from V_{B1} and V_{B2} can be obtained as follows:

$$\frac{P_{\mathrm{B1}}}{P_{\mathrm{B2}}} = \frac{V_{\mathrm{B1}}I_{\mathrm{B1}}}{V_{\mathrm{B2}}I_{\mathrm{B2}}} = \frac{V_{\mathrm{B1}}\left(\frac{V_{\mathrm{B1}}}{2L_2}D_1T_1 + I_{L2\mathrm{min}}\right)}{V_{\mathrm{B2}}\left(\frac{V_{\mathrm{B2}}}{2L_2}D_2T_2 + I_{L2\mathrm{min}}\right)}. \tag{14}$$

Substituting (11) into (14)

$$\frac{P_{\mathrm{B1}}}{P_{\mathrm{B2}}}=\frac{V_{\mathrm{B1}}\left[\frac{V_{\mathrm{B1}}}{2L_2}D_1T_1+\frac{2I_{\mathrm{Bus}}T_S-\frac{V_{\mathrm{B1}}}{L_2}D_1(1-D_1)T_1^2-\frac{V_{\mathrm{B2}}}{L_2}D_2(1-D_2)T_2^2}{2(1-D_1)T_1+2(1-D_2)T_2}\right]}{V_{\mathrm{B2}}\left[\frac{V_{\mathrm{B2}}}{2L_2}D_2T_2+\frac{2I_{\mathrm{Bus}}T_S-\frac{V_{\mathrm{B1}}}{L_2}D_1(1-D_1)T_1^2-\frac{V_{\mathrm{B2}}}{L_2}D_2(1-D_2)T_2^2}{2(1-D_1)T_1+2(1-D_2)T_2}\right]}. \tag{15}$$

From (15), the ratio of P_{B1} and P_{B2} is controlled by the magnitude of T_1 and T_2. Thus, the energy of P_{B1} and P_{B2} is allocated to the output.

F. Key Component Design

The performance of the proposed converter is highly affected by the inductance of L_1 and L_2. When V_{B2} provides energy to V_{B1} in stage I and by the charge balance rule, L_1 in boundary conduction mode (BCM) can be derived as follows:

$$L_1=\frac{D_1\left(1-D_2\right)V_{\mathrm{B2}}}{2I_{\mathrm{B1,BCM}}f_s} \tag{16}$$

where $I_{\mathrm{B1,BCM}}$ is the current with port V_{B1} under BCM.

Similarly, L_2 under BCM when V_{B1} provides energy to V_{Bus} in stage II can be derived as follows:

$$L_2=\frac{D_3\left(1-D_3\right)V_{\mathrm{B1}}}{2I_{\mathrm{Bus,BCM}}f_s} \tag{17}$$

where $I_{\mathrm{Bus,BCM}}$ is defined as the bus current under BCM.

The voltage stresses on the power switches in Stages I–III, are shown as follows:

$$V_{\mathrm{ds1}}=V_{\mathrm{ds2}}=V_{\mathrm{B1}}\quad(\text{stage I}) \tag{18}$$

$$V_{\mathrm{dsa1}}=V_{\mathrm{dsa2}}=V_{\mathrm{B1}}-V_{\mathrm{B2}}\quad(\text{stage II}) \tag{19}$$

$$V_{\mathrm{ds3}}=V_{\mathrm{ds4}}=V_{\mathrm{Bus}}\quad(\text{stage III})\,. \tag{20}$$

From V_{B2} to V_{B1} and V_{B2} to V_{Bus}, the maximum value of the current through L_1 and L_2 are, respectively, derived as the follows:

$$I_{L1\mathrm{max}}=\frac{\left(1-D_2\right)V_{\mathrm{B1}}D_2}{2L_1f_s}+\frac{|I_{\mathrm{B1}}|}{1-D_2} \tag{21}$$

$$I_{L2\mathrm{max}}=\frac{\left(1-D_3\right)V_{\mathrm{Bus}}D_3}{2L_2f_s}+\frac{I_{\mathrm{Bus}}}{1-D_3}. \tag{22}$$

The maximum current flowing through power switches S_1, S_2, S_3, S_4, and S_{a2} can be derived as

$$I_{\mathrm{S1max}}=I_{\mathrm{S2max}}=I_{L1\mathrm{max}} \tag{23}$$

$$I_{\mathrm{Sa2max}}=I_{\mathrm{S3max}}=I_{\mathrm{S4max}}=I_{L2\mathrm{max}}\,. \tag{24}$$

From V_{B1} to V_{Bus}, the maximum current through S_{a1} is derived as

$$I_{\mathrm{Sa1max}}=\frac{\left(1-D_3\right)V_{\mathrm{Bus}}D_3}{2L_2f_s}+\frac{I_{\mathrm{Bus}}}{1-D_3}. \tag{25}$$

TABLE I
SYSTEM SPECIFICATIONS AND KEY COMPONENTS

Parameters	Values
Voltage of Port 1 (V_{B1})	72 V
Voltage of Port 2 (V_{B2})	48 V
Voltage of Port 3 (V_{Bus})	200 V
Rated Power of Port 1 (P_{B1})	300 W
Rated Power of Port 2 (P_{B2})	300 W
Rated Power of Port 3 (P_{Bus})	300 W
Switching Frequency (f_s)	50 kHz
Inductances (L_1, L_2)	L_1: 130 μH L_2: 555 μH
Power MOSFETs (S_1, S_2, S_{a1}, S_{a2})	IPP110N20N3
Power MOSFETs (S_3, S_4)	SCT3080AL

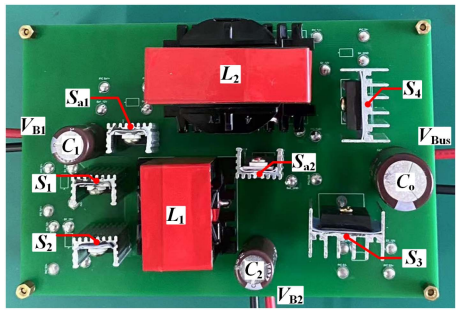

Fig. 20. Experimental prototype.

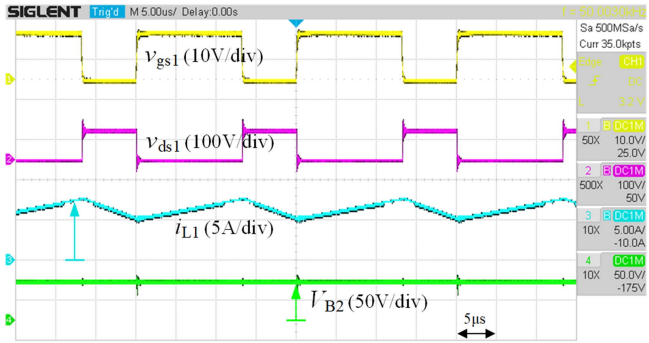

Fig. 21. Measured waveforms v_{gs1}, v_{ds1}, i_{L1}, and V_{B2} in Stage I under $P_{\mathrm{B2}}=300$ W from V_{B1} to V_{B2}.

IV. EXPERIMENT RESULTS

In a particular battery system with three ports, the battery banks have two port voltages of 72 V (port 1) and 48 V (port 2), and port 3 is a 200 V dc bus. Any two of the three ports can transfer energy to each other, and considering the voltage magnitude, any two ports are bidirectional buck/boost converters. Based on the above theoretical analysis, Fig. 15 is chosen as the topology and the laboratory prototype is built. The system specifications and key parameters are given in Table I. By setting the boundary conditions under $I_{\mathrm{B1,BCM}}=0.83$ A and $I_{\mathrm{Bus,BCM}}=0.3$ A, L_1 and L_2 are designed as 130 and 555 μH from (8) and (9), respectively. The experimental prototype is shown in Fig. 20.

In stage I under full load conditions, Figs. 21 and 22 show the measured waveforms of v_{gs1}, v_{ds1}, i_{L1}, and V_{B2} when V_{B1} provides energy to V_{B2}, and v_{gs2}, v_{ds2}, i_{L1}, and V_{B1} when V_{B2} provides energy to V_{B1}, respectively. In stage II under full load

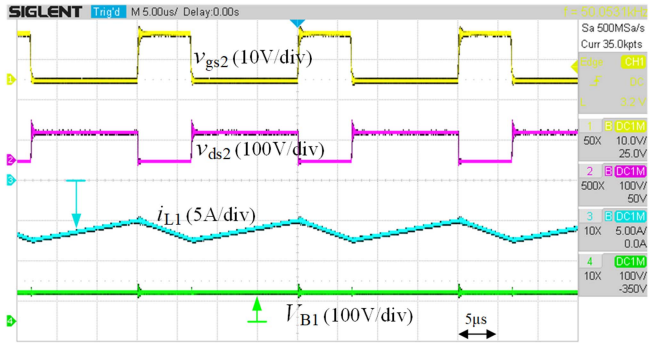

Fig. 22. Measured waveforms v_{gs2}, v_{ds2}, i_{L1}, and V_{B1} in Stage I under $P_{B1} = 300$ W from V_{B2} to V_{B1}.

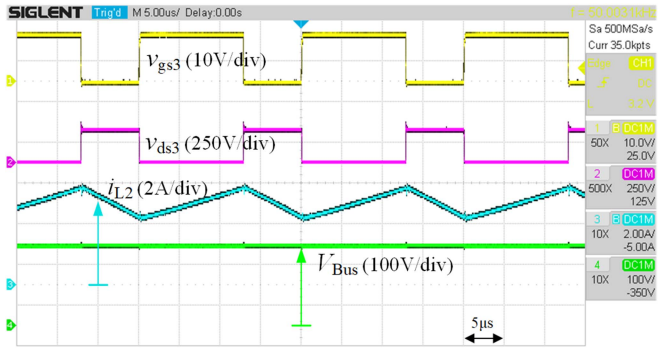

Fig. 23. Measured waveforms v_{gs3}, v_{ds3}, i_{L2}, and V_{Bus} in Stage II under $P_{Bus} = 300$ W from V_{B1} to V_{Bus}.

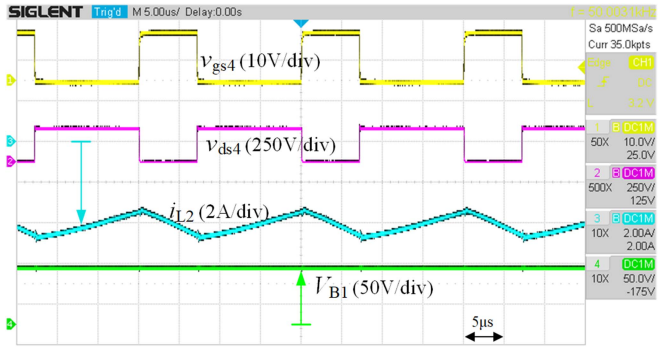

Fig. 24. Measured waveforms v_{gs4}, v_{ds4}, i_{L2}, and V_{B1} in Stage II under $P_{B1} = 300$ W from V_{Bus} to V_{B1}.

conditions, Figs. 23 and 24 show measured waveforms of v_{gs3}, v_{ds3}, i_{L2}, and V_{Bus} when V_{B1} provides energy to V_{Bus}, and v_{gs4}, v_{ds4}, i_{L2}, and V_{B1} when V_{Bus} provieds energy to V_{B1}. In stage III under full load conditions, Figs. 25 and 26 show measured waveforms of v_{gs3}, v_{ds3}, i_{L2}, and V_{Bus} when V_{B2} provides energy to V_{Bus}, and v_{gs4}, v_{ds4}, i_{L2}, and V_{B2} when V_{Bus} provides energy to V_{B2}. These experimental waveforms indicate that the proposed converter can achieve bidirectional energy transfer between any two ports. In stage IV, when V_{B2} provides energy to V_{B1} and V_{Bus}, Figs. 27 and 28 show the measured waveforms of v_{gs2}, v_{gs3}, i_{L1}, i_{L2}, v_{ds2}, V_{B1}, and V_{Bus} under $P_{B1} = 30$ W and $P_{Bus} = 270$ W, and $P_{B1} = 270$ W and $P_{Bus} = 30$ W, respectively. In Fig. 27, from V_{B2} to V_{Bus},

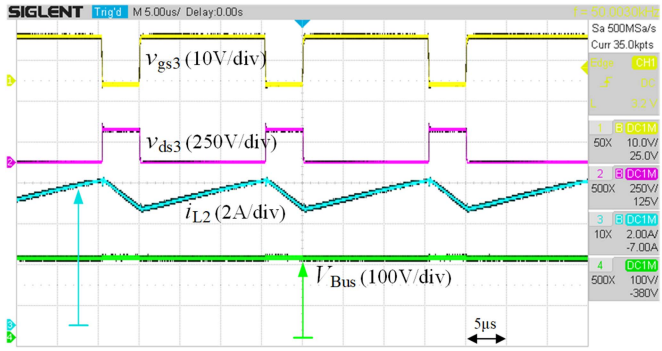

Fig. 25. Measured waveforms v_{gs3}, v_{ds3}, i_{L2}, and V_{Bus} in Stage III under $P_{Bus} = 300$ W from V_{B2} to V_{Bus}.

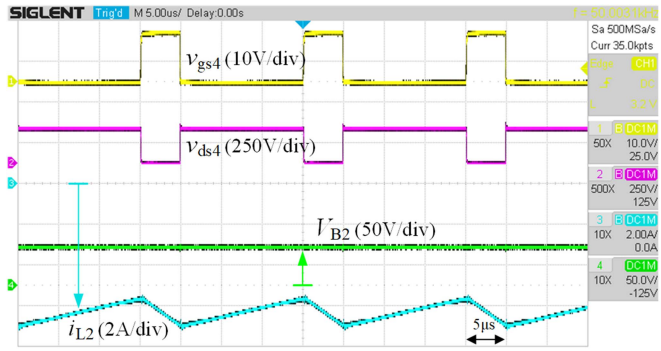

Fig. 26. Measured waveforms v_{gs4}, v_{ds4}, i_{L2}, and V_{B2} in Stage III under $P_{B2} = 300$ W from V_{Bus} to V_{B2}.

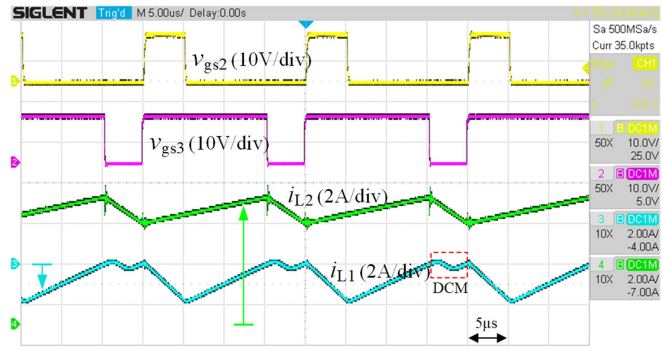

(a)

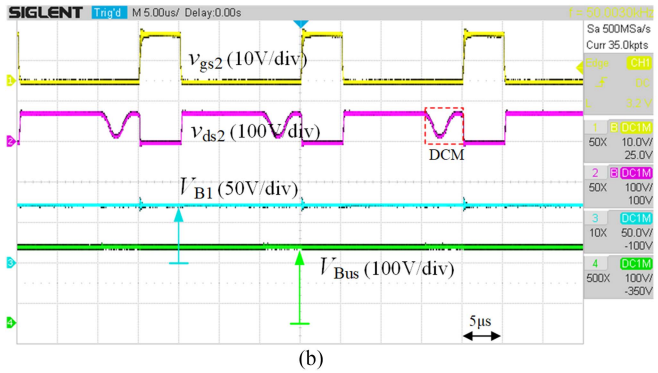

(b)

Fig. 27. Measured waveforms with (a) v_{gs2}, v_{gs3}, i_{L1}, and i_{L2} and (b) v_{gs2}, v_{ds2}, V_{B1}, and V_{Bus} in stage IV under $P_{B1} = 30$ W and $P_{Bus} = 270$ W from V_{B2} to V_{B1} and V_{Bus}.

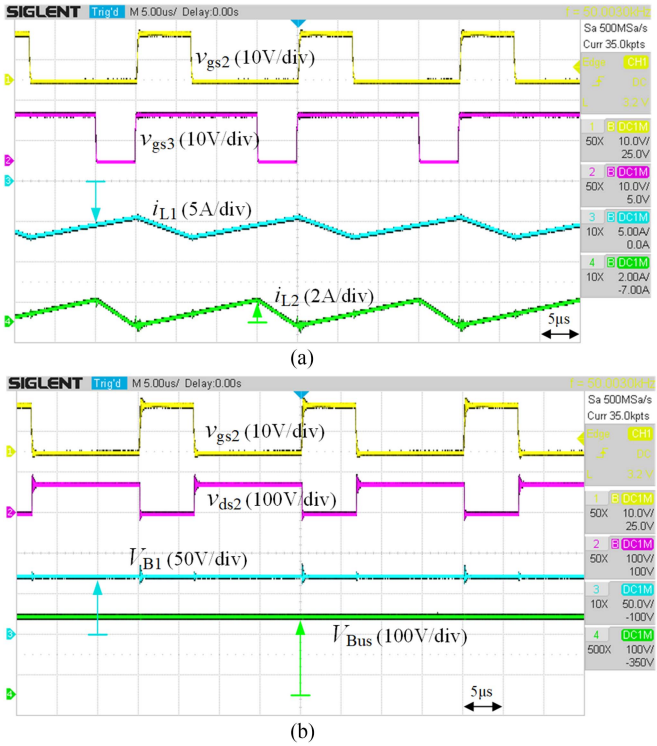

Fig. 28. Measured waveforms with (a) v_{gs2}, v_{gs3}, i_{L1}, and $i_{L2}$and (b) v_{gs2}, v_{ds2}, V_{B1}, and V_{Bus} in stage IV under $P_{B1} = 270$ W and $P_{Bus} = 30$ W from V_{B2} to V_{B1} and V_{Bus}.

after i_{L1} changes from a negative maximum value to zero, inductor L_1 resonates with the output capacitors of S_1 and S_2 due to operation in discontinuous conduction mode (DCM). The independent power flow controls of V_{B2} to V_{B1} and V_{B2} to V_{Bus} are achieved. Moreover, in Fig. 27, i_{L1} is operated in DCM); therefore, L_1 resonates with the output capacitor of S_2. Fig. 29(a) and (b) shows the measured waveforms v_{gsa1}, v_{gs3}, i_{L2}, and V_{Bus} in stage V from V_{B1} and V_{B2} to V_{Bus} under $P_{B1} = 270$ W and $P_{B2} = 30$ W, and $P_{B1} = 30$ W and $P_{B2} = 270$ W, respectively. When S_{a1} is turned ON and OFF, V_{B1} and V_{B2} transfer energy to V_{Bus} independently. By building the simulation model in MATLAB/Simulink, the mode transitions waveform is shown in Fig. 30. In SIDO mode, V_{B1} provides total power of 300 W to V_{B2} and V_{Bus}; the charging power to V_{B2} is 150 W ($i_{B2} = 3.125$ A) and the load power to V_{Bus} is also 150 W ($i_{Bus} = 0.75$ A). When load power increases to 300 W ($i_{Bus} = 1.5$ A), S_1 is turned OFF, and both V_{B1} and V_{B2} provide 150 W ($i_{B1} = 2.08$ A and $i_{B2} = 3.125$ A); then the converter changes to DISO mode.

Fig. 31 shows the measured efficiency curves of stages I–III. The power flows between V_{B1} and V_{B2} have higher efficiency, and the peak efficiency is 98.4% from V_{B1} to V_{B2}. Moreover, compared with stage II, the the increased duty cyle in stage III causes more conduction losses, decreasing the efficiency. The efficiency in DISO and SIDO modes is obtained by combining the SISO modes. For example, in SIDO mode, V_{B1} provides 30 and 270 W of energy to V_{B2} and V_{Bus}, respectively, and the efficiency 97.8% of stage I at 30 W and the efficiency 98.1% of

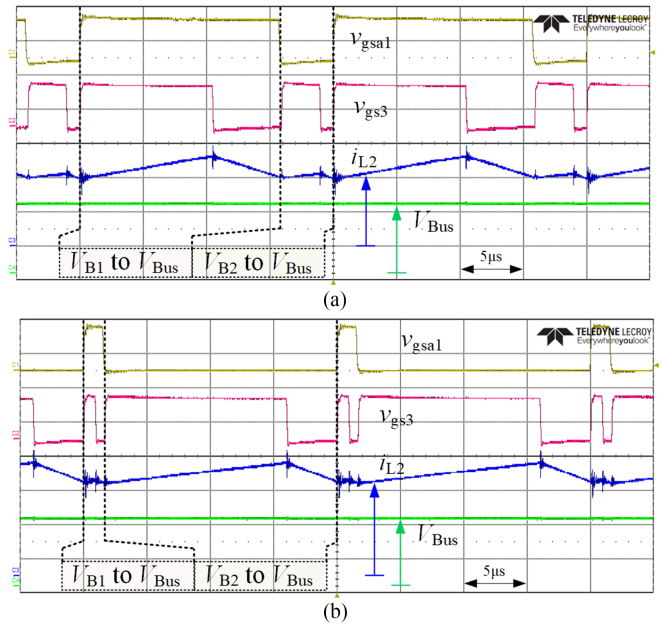

Fig. 29. Measured waveforms v_{gsa1}, v_{gs3}, i_{L2}, and V_{Bus} in stage V from V_{B1} and V_{B2} to V_{Bus} under (a) $P_{B1} = 270$ W and $P_{B2} = 30$ W and (b) $P_{B1} = 30$ W and $P_{B2} = 270$ W.

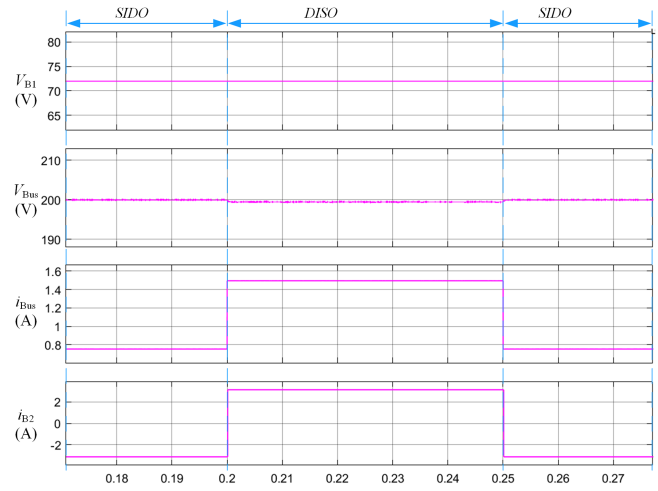

Fig. 30. Mode transitions between SIDO and DISO modes.

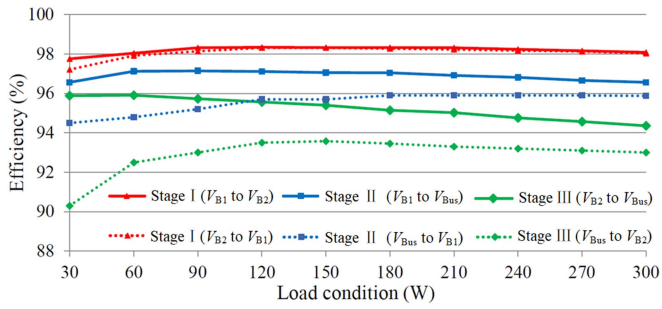

Fig. 31. Efficiency curves.

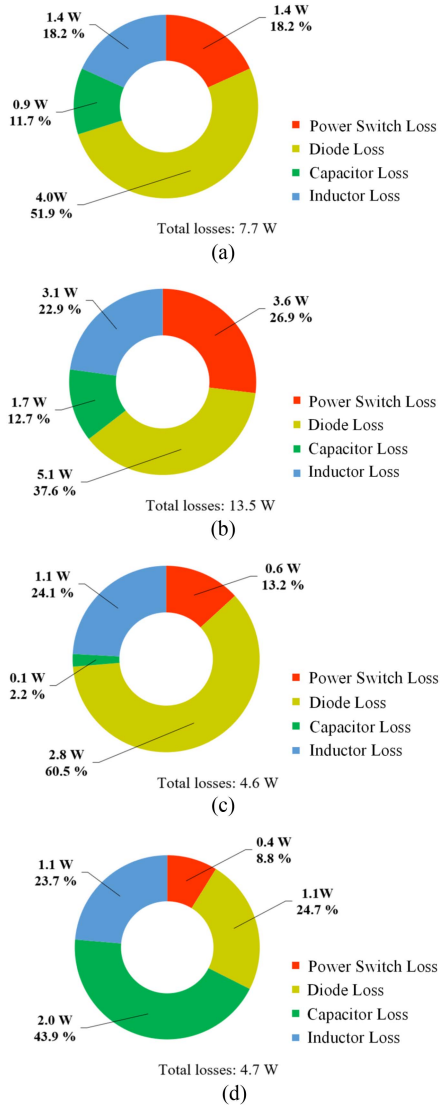

Fig. 32. Loss breakdown analyses under full load of (a) V_{B1} to V_{Bus}, (b) V_{B2} to V_{Bus}, (c) V_{B1} to V_{B2}, and (d) V_{B2} to V_{B1}.

stage II at 270 W are weighted to obtain the efficiency 98.07%; in DISO mode, when V_{B1} and V_{B2} provide 270 and 30 W of energy to V_{Bus}, respectively, the efficiency 98.1% of stage II at 270 W and the efficiency 90.4% of stage III at 30 W are weighted to obtain the efficiency 97.3%. The efficiency curves in Fig. 31 are highly affected by the boundary conditions of L_1 and L_2. Since the efficiency under step-down operation of the built BTPC is low, the boundary conditions of L_1 and L_2 are designed to obtain the highest efficiency near 50% from V_{Bus} to V_{B1} and V_{Bus} to V_{B2} load conditions. Under V_{B1} to V_{Bus}, V_{B2} to V_{Bus}, V_{B1} to V_{B2}, and V_{B2} to V_{B1}, the loss breakdown analyses of the experiments result under full load condition are shown in Fig. 32(a)–(d), respectively. Diode loss represents the antiparallel diode with current flowing through the power switch turned OFF.

V. Conclusion

To achieve systematic topology derivation for TPCs and BTPCs with independent power transferring, two systematic converter synthesis methods are proposed by adding one power switch and one diode, and two power switches, respectively. Thus, by combining the basic converters via proposed methods, a series of TPCs and BTPCs including nonisolated and isolated converters are derived. The derived converters offer benefits in terms of their simpler structures and independent power flow control. In addition, these converters can be applied in power supply systems with multiple sources or battery energy storage, such as distributed generation, hybrid electric, and fuel cell vehicles, among others—where engineers can easily obtain an appropriate architecture for specific applications. Finally, one of the nonisolated BTPCs with a common ground was analyzed and built to verify the feasibility of the proposed converter.

References

[1] Z. Q. Wang, Q. M. Luo, Y. Q. Wei, D. Mou, X. L. Lu, and P. J. Sun, "Topology analysis and review of three-port DC–DC converters," *IEEE Trans. Power Electron.*, vol. 35, no. 11, pp. 11783–11800, Nov. 2020.

[2] L. J. Chien, C. C. Chen, J. F. Chen, and Y. P. Hsieh, "Novel three-port converter with high-voltage gain," *IEEE Trans. Power Electron.*, vol. 29, no. 9, pp. 4693–4703, Sep. 2014.

[3] R. Faraji, H. Farzanehfard, G. Kampitsis, M. Mattavelli, E. Matioli, and M. Esteki, "Fully soft-switched high step-up nonisolated three-port DC-DC converter using GaN HEMTs," *IEEE Trans. Ind. Electron.*, vol. 67, no. 10, pp. 8371–8380, Oct. 2020.

[4] H. Zhu, D. Zhang, B. Zhang, and Z. Zhou, "A nonisolated three-port DC–DC converter and three-domain control method for PV-battery power systems," *IEEE Trans. Ind. Electron.*, vol. 62, no. 8, pp. 4937–4947, Aug. 2015.

[5] M. R. Al-Soeidat, H. Aljarajreh, H. A. Khawaldeh, D. D.-C. Lu, and J. G. Zhu, "A reconfigurable three-port DC–DC converter for integrated PV-battery system," *IEEE J. Emerg. Sel. Topics Ind. Electron.*, vol. 8, no. 4, pp. 3423–3433, Dec. 2020.

[6] M. Uno and K. Sugiyama, "Switched capacitor converter based multiport converter integrating bidirectional PWM and series-resonant converters for standalone photovoltaic systems," *IEEE Trans. Power Electron.*, vol. 34, no. 2, pp. 1394–1406, Feb. 2019.

[7] Y. Sato, M. Uno, and H. Nagata, "Nonisolated multiport converters based on integration of PWM converter and phase-shift-switched capacitor converter," *IEEE Trans. Power Electron.*, vol. 35, no. 1, pp. 455–470, Jan. 2020.

[8] K. Varesi, S. H. Hosseini, M. Sabahi, E. Babaei, S. Saeidabadi, and N. Vosoughi, "Design and analysis of a developed multiport high step-up DC-DC converter with reduced device count and normalized peak inverse voltage on the switches/diodes," *IEEE Trans. Power Electron.*, vol. 34, no. 6, pp. 5464–5475, Jun. 2019.

[9] Y. M. Chen, Y. C. Liu, and F. Y. Wu, "Multi-input DC/DC converter based on the multiwinding transformer for renewable energy applications," *IEEE Trans. Ind. Appl.*, vol. 38, no. 4, pp. 1096–1104, Jul./Aug. 2002.

[10] P. Bayat and A. Baghramian, "Partly isolated three-port DC-DC converter based on impedance network," *IET Power Electron.*, vol. 13, no. 11, pp. 2175–2193, Aug. 2020.

[11] T. Qian, K. Guo, and C. Qian, "A combined three-port LLC structure for adaptive power flow adjustment of PV systems," *IEEE Trans. Power Electron.*, vol. 35, no. 10, pp. 10413–10422, Oct. 2020.

[12] X. Sun, Y. Shen, W. Li, and H. Wu, "A PWM and PFM hybrid modulated three-port converter for a standalone PV/battery power system," *IEEE J. Emerg. Sel. Topics Ind. Electron.*, vol. 3, no. 4, pp. 984–1000, Dec. 2015.

[13] J. Zhang et al., "A three-port LLC resonant DC/DC converter," *IEEE J. Emerg. Sel. Topics Ind. Electron.*, vol. 7, no. 4, pp. 2513–2524, Dec. 2019.

[14] M. Uno, R. Oyama, and K. Sugiyama, "Partially isolated single-magnetic multiport converter based on integration of series-resonant converter and bidirectional PWM converter," *IEEE Trans. Power Electron.*, vol. 33, no. 11, pp. 9575–9587, Nov. 2018.

[15] Y. H. Hu, W. D. Xiao, W. P. Cao, B. Ji, and D. J. Morrow, "Three-port DC-DC converter for stand-alone photovoltaic systems," *IEEE Trans. Power Electron.*, vol. 30, no. 6, pp. 3068–3076, Jun. 2015.

[16] H. Tao, A. Kotsopoulos, J. L. Duarte, and M. A. M. Hendrix, "A soft-switched three-port bidirectional converter for fuel cell and supercapacitor applications," in *Proc. IEEE 36th Power Electron. Specialists Conf.*, 2005, pp. 2487–2493.

[17] M. Kumar, P. M. Barbosa, J. M. Ruiz, J. Minli, and S. Hao, "Isolated three-port bidirectional DC–DC converter for electric vehicle applications," in *Proc. IEEE Appl. Power Electron. Conf. Expo.*, 2022, pp. 2000–2007.
[18] J. Schafer and J. W. Kolar, "Three-port series-resonant DC/DC converter for automotive charging applications," *Electronics*, vol. 10, no. 20, p. 2543, Oct. 2021.
[19] S. Mukherjee, D. Mukherjee, and D. Kastha, "Multiport soft-switching bidirectional DC–DC converter for hybrid energy storage systems," in *Proc. IEEE Appl. Power Electron. Conf. Expo.*, 2019, pp. 2103–2109.
[20] A. K. Bhattacharjee, N. Kutkut, and I. Batarseh, "Review of multiport converters for solar and energy storage integration," *IEEE Trans. Power Electron.*, vol. 34, no. 2, pp. 1431–1445, Feb. 2019.
[21] V. Monteiro, J. G. Pinto, and J. L. Afonso, "Experimental validation of a three-port integrated topology to interface electric vehicles and renewables with the electrical grid," *IEEE Trans. Ind. Inform.*, vol. 14, no. 6, pp. 2364–2374, Jun. 2018.
[22] I. Askarian, M. Pahlevani, and A. M. Knight, "Three-port bidirectional DC/DC converter for DC nanogrids," *IEEE Trans. Power Electron.*, vol. 36, no. 7, pp. 8000–8011, Jul. 2021.
[23] H. Aljarajreh, D. D.-C. Lu, Y. P. Siwakoti, R. P. Aguilera, and C. K. Tse, "A method of seamless transitions between different operating modes for three-port DC-DC converters," *IEEE Access*, vol. 9, pp. 59184–59195, 2021.
[24] A. Hintz, U. R. Prasanna, and K. Rajashekara, "Novel modular multiple-input bidirectional DC–DC power converter (MIPC) for HEV/FCV application," *IEEE Trans. Ind. Electron.*, vol. 62, no. 5, pp. 3163–3172, May 2015.
[25] E. C. dos Santos, "Dual-output DC–DC buck converters with bidirectional and unidirectional characteristics," *IET Power Electron.*, vol. 6, no. 5, pp. 999–1009, May 2013.
[26] T. Bhattacharya, V. S. Giri, K. Mathew, and L. Umanand, "Multiphase bidirectional flyback converter topology for hybrid electric vehicles," *IEEE Trans. Ind. Electron.*, vol. 56, no. 1, pp. 78–84, Jan. 2009.
[27] C. H. Zhao, S. D. Round, and J. W. Kolar, "An isolated three-port bidirectional DC–DC converter with decoupled power flow management," *IEEE Trans. Power Electron.*, vol. 23, no. 5, pp. 2443–2453, Sep. 2008.
[28] H. Krishnaswami and N. Mohan, "Three-port series-resonant DC–DC converter to interface renewable energy sources with bidirectional load and energy storage ports," *IEEE Trans. Power Electron.*, vol. 24, no. 10, pp. 2289–2297, Oct. 2009.
[29] X. Tang, H. Wu, W. Hua, Z. Yu, and Y. Xing, "Three-port bidirectional series-resonant converter with first-harmonic-synchronized PWM," *IEEE J. Emerg. Sel. Topics Power Electron.*, vol. 9, no. 2, pp. 1410–1419, Apr. 2021.
[30] J. L. Duarte, M. Hendrix, and M. G. Simoes, "Three-port bidirectional converter for hybrid fuel cell systems," *IEEE Trans. Power Electron.*, vol. 22, no. 2, pp. 480–487, Mar. 2007.
[31] Y. E. Wu and I. C. Chen, "Novel integrated three-port bidirectional DC/DC converter for energy storage system," *IEEE Access*, vol. 7, pp. 104601–104612, 2019.
[32] H. F. Wu, K. Sun, S. Ding, and Y. Xing, "Topology derivation of non-isolated three-port DC–DC converters from DIC and DOC," *IEEE Trans. Power Electron.*, vol. 28, no. 7, pp. 3297–3307, Jul. 2013.
[33] Q. Tian, G. Zhou, R. Liu, X. Zhang, and M. Leng, "Topology synthesis of a family of integrated three-port converters for renewable energy system applications," *IEEE Trans. Ind. Electron.*, vol. 68, no. 7, pp. 5833–5846, Jul. 2021.
[34] Y. C. Liu and Y. M. Chen, "A systematic approach to synthesizing multi-input DC–DC converters," *IEEE Trans. Power Electron.*, vol. 24, no. 1-2, pp. 116–127, Jan. 2009.
[35] Y. Li, X. Ruan, D. Yang, F. Liu, and C. K. Tse, "Synthesis of multiple-input DC/DC converters," *IEEE Trans. Power Electron.*, vol. 25, no. 9, pp. 2372–2385, Sep. 2010.
[36] G. Chen, Z. Jin, Y. Deng, X. He, and X. Qing, "Principle and topology synthesis of integrated single-input dual-output and dual-input single-output DC–DC converters," *IEEE Trans. Ind. Electron.*, vol. 65, no. 5, pp. 3815–3825, May 2018.
[37] G. Chen, Y. Liu, X. Qing, M. Ma, and Z. Lin, "Principle and topology derivation of single-inductor multi-input multi-output DC–DC converters," *IEEE Trans. Ind. Electron.*, vol. 68, no. 1, pp. 25–36, Jan. 2021.
[38] G. Chen, Y. Liu, X. Qing, and F. Wang, "Synthesis of integrated multiport DC–DC converters with reduced switches," *IEEE Trans. Ind. Electron.*, vol. 67, no. 6, pp. 4536–4546, Jun. 2020.
[39] H. Moradisizkoohi, N. Elsayad, and O. A. Mohammed, "A family of three-port three-level converter based on asymmetrical bidirectional half-bridge topology for fuel cell electric vehicle applications," *IEEE Trans. Power Electron.*, vol. 34, no. 12, pp. 11706–11724, Dec. 2019.
[40] T. J. Liang, P. Luo, and K. H. Chen, "A high step-up DC–DC converter with three-winding coupled inductor for sustainable energy systems," *IEEE Trans. Ind. Electron.*, vol. 69, no. 10, pp. 10249–10258, Oct. 2022.
[41] K. Zaoskoufis and E. C. Tatakis, "Isolated ZVS-ZCS DC–DC high step-up converter with low-ripple input current," *IEEE J. Emerg. Sel. Topics Ind. Electron.*, vol. 2, no. 4, pp. 464–480, Oct. 2021.
[42] G. Chen, Y. S. Lee, S. Y. R. Hui, D. Xu, and Y. Wang, "Actively clamped bidirectional flyback converter," *IEEE Trans. Ind. Electron.*, vol. 47, no. 4, pp. 770–779, Aug. 2000.

Peng Luo was born in China. He received the M.S. degree in electrical engineering from the China University of Mining and Technology, Xuzhou, China, in 2015, and the Ph.D. degree in electrical engineering from National Cheng Kung University, Tainan, Taiwan, in 2023.

He is currently a Lecturer with Guangdong Ocean University, Zhanjiang, China. His research interests include power electronics converters and energy conversion.

Tsorng-Juu Liang (Fellow, IEEE) received the M.S. and Ph.D. degrees in electrical engineering from the University of Missouri, Columbia, MI, USA, in 1990 and 1993, respectively.

He is currently a Distinguished Professor with National Cheng Kung University (NCKU), Tainan, Taiwan. He is currently an Associate Dean of the College of Electrical Engineering and Computer Science and the Director of Green Energy Electronics Research Center, NCKU. His research interests include power IC design, high-efficiency power converters, high-efficiency lighting systems, and renewable energy conversion.

Dr. Liang is an Associate Editor for IEEE TRANSACTIONS ON POWER ELECTRONICS, the Editor-in-Chief of IEEE JOURNAL OF EMERGING AND SELECTED TOPICS IN POWER ELECTRONICS, the BoG of Taiwan Power Electronics Association, and the BoG of the Chinese Institute of Electrical Engineering, Kaohsiung Branch. From 2014 to 2015, he was the Distinguished Lecturer of IEEE Circuits and System Society. He was the Board of Directors of Catcher Technology, Taiwan, Compucase Enterprise, Taiwan, EpiLED, Taiwan, and Leadtrend Technology, Taiwan, and the Chair of IEEE Tainan Section and the Technical Committee TC6 Chair of IEEE Power Electronics Society. He was also the Organizing Committee Member of IEEE International Future Energy Electronics Conference in 2013 and 2015, and the General Chair of IFEEC2017-ECCE Asia. In 2015, he was the recipient of the Outstanding Professor Award from Chinese Institute of Engineering and the Outstanding Contributions Award from Taiwan Power Electronics Association in 2018.

Kai-Hui Chen was born in Kaohsiung, Taiwan, in 1984. He received the B.S. and Ph.D. degrees in electrical engineering from the National Cheng Kung University, Tainan, Taiwan, in 2007 and 2017, respectively.

He was with Green Energy Project Office, National Applied Research Laboratories, Taiwan. He is currently a Postdoctoral Researcher with National Cheng Kung University. His current research interests include power converter analysis, power converter control circuit design, control system design, and power ICs.

Shih-Ming Chen was born in Tainan, Taiwan. He received the B.S. and Ph.D. degrees in electrical engineering from National Cheng Kung University (NCKU), Tainan, Taiwan, in 2003 and 2011, respectively.

From 1993 to 2019, he was an Engineer with R&D Center and a Manager with several Taiwan power supply companies (e.g., Delta, Lite-ON). His product development experience ranges from uninterrupted power supplies (offline/online/interactive), desktop PC power supplies (ATX), electric bike chargers, electric ballasts (T5), LCD backlight inverters (CCFL) and TV system power supply (LED), photovoltaic Inverters (Solar microinverter), server power supplies, and the data center power system. From 2019 to 2020, he was a Visiting Scholar with the Center for Power Electronics System, Virginia Tech, Blacksburg, VA, USA. Since 2021, he has been with Green Energy Electronics Research Center, NCKU for postdoctoral research. His research interests include ac/dc, dc/dc, and dc/ac converters, photovoltaic inverter, switching power supply, uninterrupted power system, and HVDC power system.

Jiann-Fuh Chen (Fellow, IEEE) received the B.S., M.S., and Ph.D. degrees in electrical engineering from National Cheng Kung University (NCKU), Tainan, Taiwan, in 1978, 1980, and 1985, respectively.

He is currently a Distinguished Professor of electrical engineering with NCKU. From 2016 to 2021, he was the Vice Dean of the College of Electrical Engineering and Computer Science. From 2013 to 2015, he was an Associate Vice President of the Office of Research and Development, NCKU. He was also the Chairman of Taiwan Power Electronics Association and the Governor of Kaohsiung Section, Chinese Institute of Electrical Engineering, Beijing, China. From 2010 to 2012, he was also a Convener with Electrical Power Program, National Science Council (NSC), Taiwan. From 1996 to 1999, he was with NCKU in various capacities that include the Director of Electrical Laboratories. From 1998 to 2000, he was a Manager with the Business Section, Research and Services Headquarter. From 2000 to 2001, he was a Supervisor with Engineering Division Section, National Cheng Kung Hospital, Tainan, Taiwan. From 2003 to 2006, he was the Director of Business Incubator Center, Taipei, Taiwan. From 2008 to 2011, he was the Chairman of Electrical Engineering Department. He leads more than 30 research projects sponsored by MOST Taiwan. He authored or coauthored one book, more than 96 journal articles, 143 conference papers, and holds 40 patents. His research interests include high voltage, high power and high-efficiency conversion technology, renewable energy conversion technology, power system, and lighting technology.

Dr. Chen was the recipient of the CIE Outstanding Engineering Professor Award 2016 and TaiPEA Outstanding Contribution for Power Electronic Award 2019.